ACS SENSORS

pubs.acs.org/acssensors Article

Development of a Rapid and Sensitive CasRx-Based Diagnostic Assay for SARS-CoV-2

Daniel J. Brogan,[○] Duverney Chaverra-Rodriguez,[○] Calvin P. Lin,[○] Andrea L. Smidler,[▽] Ting Yang,[▽] Lenissa M. Alcantara, Igor Antoshechkin, Junru Liu, Robyn R. Raban, Pedro Belda-Ferre, Rob Knight, Elizabeth A. Komives, and Omar S. Akbari*

Cite This: https://doi.org/10.1021/acssensors.1c01088 Read Online

ACCESS | Metrics & More | Article Recommendations | Supporting Information

ABSTRACT: The development of an extensive toolkit for potential point-of-care diagnostics that is expeditiously adaptable to new emerging pathogens is of critical public health importance. Recently, a number of novel CRISPR-based diagnostics have been developed to detect SARS-CoV-2. Herein, we outline the development of an alternative CRISPR nucleic acid diagnostic utilizing a Cas13d ribonuclease derived from *Ruminococcus flavefaciens* XPD3002 (CasRx) to detect SARS-CoV-2, an approach we term SENSR (sensitive enzymatic nucleic acid sequence reporter) that can detect attomolar concentrations of SARS-CoV-2. We demonstrate 100% sensitivity in patient-derived samples by lateral flow and fluorescence readout with a detection limit of 45 copy/μL. This technology expands the available nucleic acid diagnostic toolkit, which can be adapted to combat future pandemics.

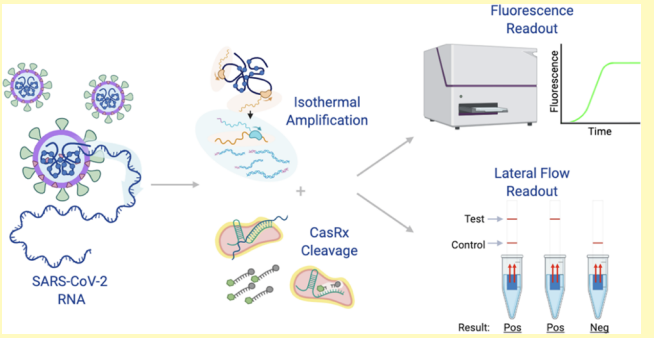

KEYWORDS: *COVID-19, CRISPR, Cas13d, nucleic acid diagnostic, isothermal*

Following emergence from China in late 2019,[1−3] severe acute respiratory syndrome coronavirus 2 (SARS-CoV-2)[1,4] has spread to almost every country despite unprecedented control efforts.[5] Compared to H1N1, Ebola, MERS, and SARS-CoV-1 outbreaks, this novel coronavirus represents the first pandemic characterized by widespread global transmission coupled with significant mortality. Robust identification and isolation of all infected individuals are essential for curtailing disease transmission. The ongoing SARS-CoV-2 pandemic presents an unparalleled global public health emergency, which spurred the urgent development of molecular diagnostics and therapeutics for timely patient identification, isolation, and treatment. The economic, health, and societal damage wrought by SARS-CoV-2 highlights the importance of expanding and improving on current diagnostic technologies to identify and prevent future pandemics.

Detection of nucleic acids from pathogens is typically accomplished using real-time polymerase chain reaction (RT-qPCR) methodologies. RT-qPCR diagnostics are highly specific and sensitive, detecting nucleic acids consistently at low copy numbers.[6] However, these diagnostics are often time-consuming and require specialized laboratory equipment, limiting the ability to expand RT-qPCR diagnostics into point-of-care settings.[7] Therefore, alternative technologies with the potential to yield cost- and time-effective point-of-care diagnostics demand investment.

CRISPR-Cas nucleases can be easily programmed to target nucleic acids in a sequence-specific manner,[8−10] making them prime candidates for the detection and diagnosis of genetic material and therefore comprise the CRISPR diagnostics (CRISPRDx) pipeline.[11−14] These systems rely on Type II Cas enzymes to physically bind target sequences[15] or collateral cleavage by Type V or Type VI nucleases to detect DNA[13,14,16] or RNA species, respectively.[11,12,17] Since the pandemic onset, an array of innovative diagnostics and prophylactics relying on these effectors have been adapted to detect or target SARS-CoV-2 with unprecedented speed,[15,18−29] most notably represented by the DETECTR (DNA endonuclease-targeted CRISPR trans reporter)[13,14] and SHERLOCK (specific high-sensitivity enzymatic reporter unLOCKing)[11,12] systems (summarized in Figure S1, Table S1). To maximize all of the capabilities of and expand the CRISPRDx toolkit, it is important to evaluate all Cas enzymes that can complement or supplement existing systems.

Similar to Cas ribonucleases used in CRISPRDx systems, Cas13d effectors, such as RfxCas13d (CasRx), exclusively target

Received: May 26, 2021
Accepted: October 14, 2021

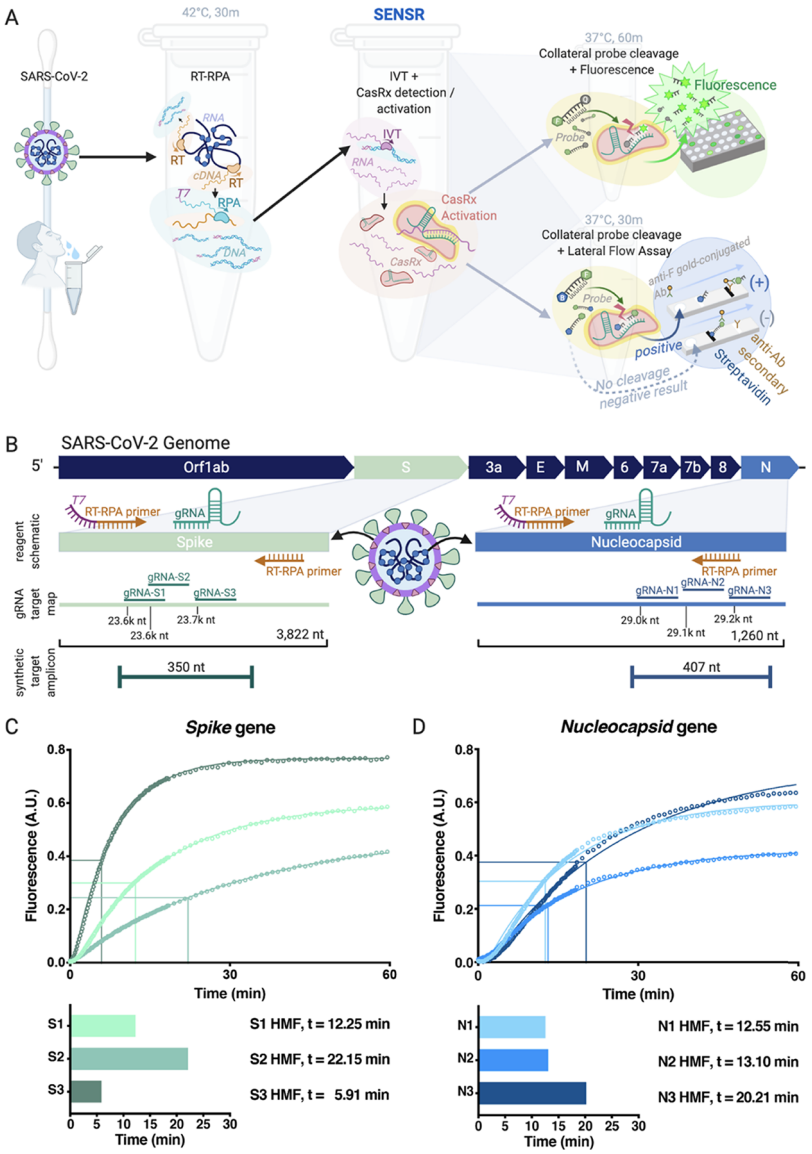

Figure 1. Harnessing SENSR to detect evidence of SARS-CoV-2 viral transcripts. (A) Overview of assay workflow. Following extraction of viral RNA, the detection protocol requires two distinct reactions, and the readout may be performed in two different methods: fluorescence or lateral flow. In the first reaction, specific target sequences within the viral RNA are reverse transcribed (RT) into cDNA and amplified by RPA at 42 °C for 30 min. During amplification, a T7 promoter is incorporated into the 5′ terminus of the amplicons (T7, purple). In the next reaction, both *in vitro* transcription (IVT) and CasRx collateral cleavage occur simultaneously (pink). Recognition and cleavage of the target RNA sequence (purple) complementary to the gRNA (emerald) induce collateral cleavage of bystander RNA molecules. Collateral cleavage of a modified probe conjugated to 6-FAM, and a fluorescence quencher facilitates readout by fluorescence (top right). Collateral cleavage of a modified probe conjugated to 6-FAM, and biotin facilitates readout by lateral flow assay (bottom right). (B) Schematic of the SARS-CoV-2 genome, RPA reagents, gRNA target sites, and synthetic amplicon position. The S (*Spike*) and N (*Nucleocapsid*) genes are enlarged to depict the design schematic in more detail (sage and blue, respectively). The schematic depicts the relative position of the RT-RPA primers and gRNAs used in the amplification and cleavage reactions, respectively. The gRNA target map outlines all six gRNAs tested through the course of this work, with their relative positions. The S-gene is 3822 nt in length, while the N-gene is 1260 nt in length. Synthetic target amplicon denotes the length of the synthetic viral genome fragment used in SENSR assays and its relative position within the gene coding sequence. (C) Preliminary characterization of S-targeting gRNAs (gRNA-S1, -S2, and -S3) in a SENSR fluorescence assay. Synthetic *Spike* gene templates (10 000 copy/μL) were subjected to RT-RPA for each respective gRNA tested and then transferred into a CCR. Data were acquired for 60 min and plotted by normalizing individual experimental data points to averaged data of controls at each time point. Half-maximum fluorescence (HMF) was then calculated to determine which gRNA resulted in the fastest cleavage of the fluorescent probe. Intersecting lines represent the location of HMF for each group. (D) Preliminary characterization of N-targeting gRNAs (gRNA-N1, -N2, and -N3) in a SENSR fluorescence assay. Synthetic *Nucleocapsid* gene templates (10 000 copy/μL) were subjected to RT-RPA for each respective gRNA tested and then transferred into a CCR. Data were acquired, plotted, and analyzed identical to the method described for S-targeting guides. Intersecting lines represent the location of HMF for each group.

RNA species and possess target-dependent collateral cleavage activity.[30−32] Cas13d enzymes do not require a protospacer flanking sequence (PFS),[9,30,32,33] thus presenting an advantage for flexible targeting. While the genetic modulatory effects of CasRx have been thoroughly characterized in *Drosophila*, *zebrafish*, and human cells,[30,31,34,35] and its putative prophylactic properties against SARS-CoV-2 have been demonstrated,[25] its potential as a diagnostic system has not yet been explored.

https://doi.org/10.1021/acssensors.1c01088
ACS Sens. XXXX, XXX, XXX−XXX

Herein, we report the first use of CasRx as a molecular diagnostic, developing a unique system we term SENSR (sensitive enzymatic nucleic acid sequence reporter) and demonstrate robust detection of SARS-CoV-2 viral sequences. We exploit the collateral cleavage activity of CasRx to detect SARS-CoV-2 in both synthetic templates as well as in patient-derived samples via fluorescence and paper-based LF readouts. To maximize specificity, we performed an extensive bioinformatic analysis to identify novel conserved and specific viral targets to minimize false-negative and false-positive rates, respectively. We demonstrate that within a detection limit of 45 copy/μL, SENSR exhibits 100% sensitivity by both fluorescence and LF readouts, detecting SARS-CoV-2 in 60 min or less total reaction time. The detection limit of SENSR is comparable to previously established CRISPRDx systems,[20,23,2420,23,24] and the system presents promise for improvement.

RESULTS

SENSR Workflow. Derived from protocols originally developed for (Figure S1, Table S1) Cas13a and Cas13b,[11,12,20,33] we established a two-step nucleic acid detection protocol using recombinant CasRx (Figure S2). Target sequences are first amplified in a 30 min isothermal preamplification reaction by combining reverse transcription with recombinase polymerase amplification (RT-RPA).[36] The RT-RPA reaction produces numerous dsDNA amplicons containing a gRNA target site and an upstream T7 promoter sequence. Next, the RT-RPA reaction is transferred into a second reaction, termed CasRx cleavage reaction (CCR), containing a T7 polymerase and the CasRx ribonucleoprotein. In the CCR, the dsDNA amplicons are transcribed into ssRNA molecules to be cleaved by CasRx. This initial cleavage event initiates the collateral cleavage activity of CasRx, resulting in the cleavage of a bystander ssRNA probe. Collateral cleavage of the probe is analyzed by either fluorescence or lateral flow (LF) readouts, thus indicating the presence or absence of SARS-CoV-2 genomic sequences (Figures 1A and S3).

Target Selection and Validation. Diagnostics require high specificity to limit the probability of false positives from the detection of random nucleic acids. To ensure the specificity of our target sites, we established a bioinformatic pipeline and searched for 30 nt sequences conserved across the first 433 published SARS-CoV-2 genomes (available at Genbank on April 7th, 2020) and without homology to other coronaviruses (ViPR, Virus Pathogen Resource, $n = 3164$). This search yielded a panel of gRNA target sites ($n = 8846$) less likely to result in false positives or negatives due to sequence constraints (Figure S4, Tables S2 and S3). Aligning with previously established diagnostics, we selected the *Spike* (S) and *Nucleocapsid* (N) genes as the targets of SENSR for system validation.[20,23,37,38] The bioinformatic analysis revealed multiple specific sequences within the S-gene ($n = 1568$) and the N-gene ($n = 150$), to which we designed three guides for each gene (S: gRNA-S1, -S2, -S3; N: gRNA-N1, -N2, -N3) (Figure 1B, Tables S2 and S4). To validate these gRNAs against SARS-CoV-2, we generated synthetic ssRNA gene fragments mimicking portions of the *Spike* and *Nucleocapsid* genomic sequences (Figure 1B, Table S4) and assessed CasRx cleavage activity *in vitro*. Initial characterization of on-target cleavage revealed degradation of target transcripts for all guides tested (Figure S5A,B), motivating further assessment of all candidates.

To select the best candidate for each target gene, we tested each gRNA in a preliminary SENSR fluorescence reaction (Figure 1A) against a high-copy number of synthetic template (10 000 copy/μL). Fluorescence data acquired were then analyzed to determine the time each gRNA reached its half-maximum fluorescence (HMF). HMF values were calculated by fitting a nonlinear regression to the fluorescence data acquired over 1 h. The equation for the nonlinear regression was then used to solve for the time HMF occurred (see Supporting Information). From the analysis, gRNA-S3 ($t = 5.91$ min) of the S-targeting group and gRNA-N1 ($t = 12.55$ min) of the N-targeting group resulted in the fastest HMF times and were selected for downstream analysis (Figure 1C,D).

Optimization of SENSR. We and others have recently demonstrated that on-target cleavage activates a secondary collateral cleavage property of CasRx.[30,31,34] We sought to exploit the collateral cleavage activity of CasRx to cleave a bystander fluorescent probe in trans, facilitating detection of SARS-CoV-2 by fluorimetry (Figure S3). A previous study has demonstrated that each Cas13 enzyme exhibits select di-nucleotide sequence preferences for collateral cleavage;[12] however, no such analysis has been performed on CasRx. To develop a probe cleavable by CasRx, we generated ten custom 6 nucleotide ssRNA probes, with variable di-nucleotide sequences, each conjugated to a 5′ fluorescent molecule (6-FAM) and a 3′ fluorescence quencher (FQ), whereupon separation following cleavage results in detectable fluorescence signal (Figure S6A, Table S4). Following the incubation of CasRx with gRNA-N1 in the presence or absence of the synthetic N-gene, the poly-U and CU/UC probes yielded significant and detectable fluorescence compared to the no-template control (NTC) (poly-U and CU/UC: $p < 0.0001$). However, the fluorescence signal increase over noise in the poly-U group was significantly higher than that of the CU/UC group ($p < 0.0001$), suggesting a preference for poly-U stretches by CasRx and motivating the use of the poly-U probe in the remainder of the experiments (Figure S6B,C, Table S4).

Following probe selection, we set to optimize the SENSR reaction conditions for the amplification and cleavage reactions. We first evaluated how varying the volume of sample input into the RT-RPA reaction affected the detection of a target. To do so, we diluted the synthetic *Nucleocapsid* template to 1000 copy/μL and added the templates to the RT-RPA reaction at 10, 20, 28.5, 39, 47, and 52% v/v (Table S5). After amplification, the samples were then transferred to the CCR and targeted by gRNA-N1. From the analysis, we found the 28.5% volume input group resulted in the fastest detection time compared to all other conditions tested (HMF = 7.85 min) and selected 28.5% sample input as our optimized condition (Figure S7A,B). We next set out to determine how varying the volume of RT-RPA transferred into the CCR influenced the speed of detection. We accomplished this by amplifying 1000 copy/μL of the synthetic *Nucleocapsid* template, transferring varied volumes of RT-RPA into the CCR, and targeting the amplicons with gRNA-N3 (Table S6). From the analysis, we found that 1 and 10 μL RT-RPA volume added resulted in the two fastest detection times, respectively (1 μL: HMF = 19.23 min; 10 μL: HMF = 30.3 min) (Figure S7C). However, upon further analysis, we found 1 μL RT-RPA volume added resulted in significantly lower signal over noise compared to 5, 7.5, and 10 μL volume added (5 μL: $p = 0.0131$, 7.5 μL: $p = 0.0021$, 10 μL: $p = 0.0001$) (Figure S7D). We therefore selected 10 μL RT-RPA volume added as our optimized condition for a standard protocol.

In an effort to identify the optimal time to detection for SENSR, we further evaluated the system by varying the

https://doi.org/10.1021/acssensors.1c01088
ACS Sens. XXXX, XXX, XXX−XXX

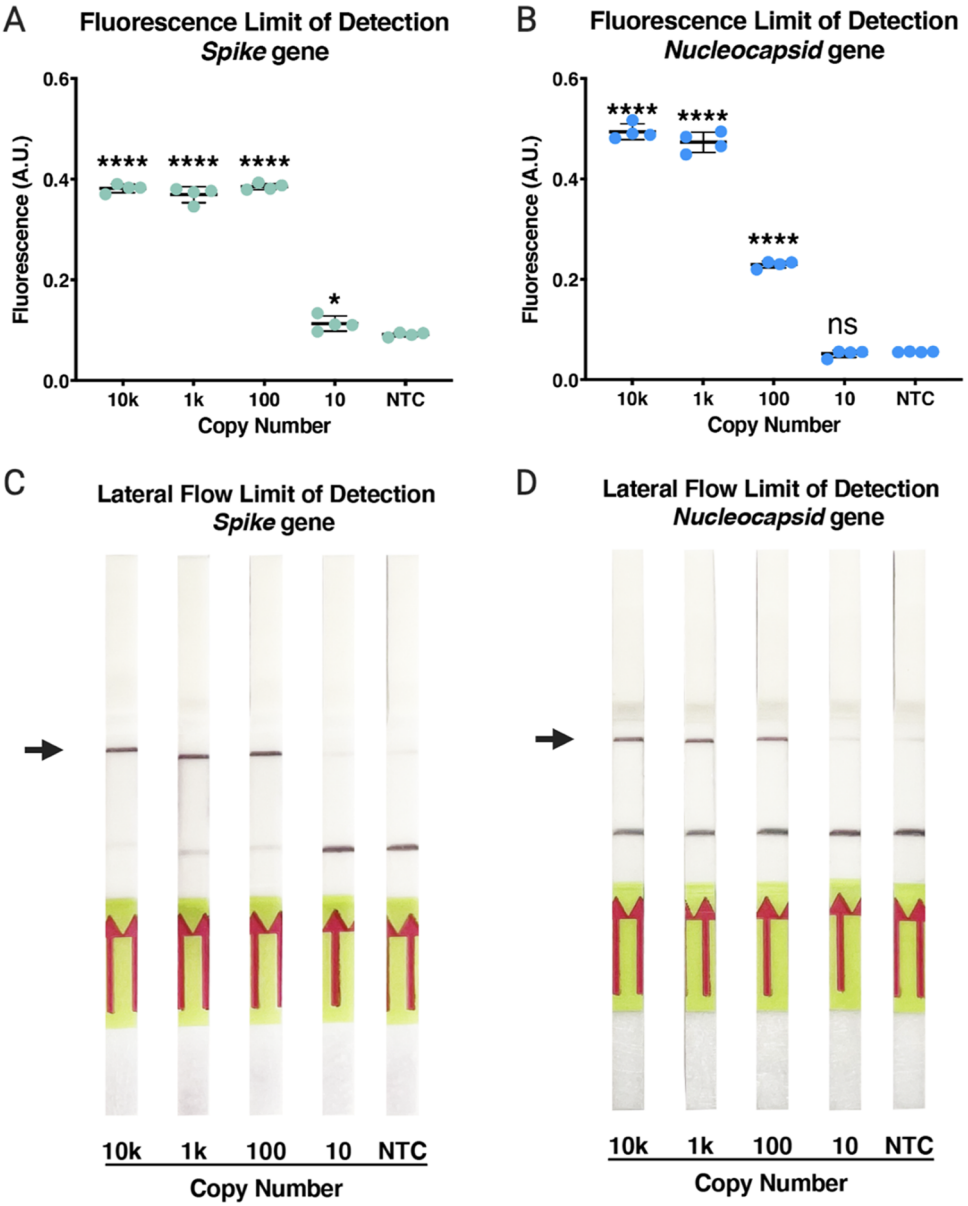

Figure 2. SARS-CoV-2 detection by SENSR via fluorescence and lateral flow assay. (A) Analysis of the limit of detection (LoD) for gRNA-S3 targeting the *Spike* gene. Synthetic S-gene templates were diluted on a logarithmic scale from 10 000 to 10 copy/μL. The fluorescence signal plotted represents the fluorescence signal* at 60 min subtracted by the initial fluorescence signal recorded. A.U.; arbitrary units. Data represents mean ± SD from quadruplicate measurements. Significance is representative of Dunnett's multiple comparisons test for experimentals compared to NTC (10 000, 1000, 100) $p < 0.0001$, (10) $p = 0.0461$. (B) Analysis of the limit of detection (LoD) for gRNA-N1 targeting the *Nucleocapsid* gene. Synthetic N-gene templates were diluted on a logarithmic scale from 10 000 to 10 copy/μL. The fluorescence signal plotted represents the final data acquired at 60 min subtracted by the initial fluorescence signal recorded. A.U.; arbitrary units. Data represents mean ± SD from quadruplicate measurements. Significance is representative of Dunnett's multiple comparisons test for experimentals compared to NTC (10 000, 1000, 100) $p < 0.0001$. (C) LoD analysis of lateral flow (LF) for gRNA-S3 targeting the *Spike* gene. Synthetic S-gene templates were diluted on a logarithmic scale from 10 000 to 10 copy/μL. CasRx detection reaction incubated for 30 min prior to addition of dipstick and imaging results. Positive results were indicated by increased saturation of the top band (arrow). (D) LoD analysis of lateral flow (LF) for gRNA-N1 targeting the *Nucleocapsid* gene. Synthetic N-gene templates were diluted on a logarithmic scale from 10 000 to 10 copy/μL. CasRx detection reaction incubated for 30 min prior to addition of dipstick and imaging results. Positive results were indicated by increased saturation of the top band (arrow).

amplification time and assessing the effect on time to detection. We tested three different amplification times (15, 30, and 45 min) using the best candidate guides identified in the preliminary analysis (gRNA-S3 and gRNA-N1). From the analysis, we observed that gRNA-S3 resulted in rapid detection regardless of amplification time, where the 30 min amplification group demonstrated the fastest detection time tested (HMF = 4.22 min) (Figure S8A). We also found that the fastest detection time for gRNA-N1 was after 30 min of amplification (HMF = 13.25 min) (Figure S8B). To confirm that 30 min is the best amplification time regardless of the gRNA used, we further evaluated the fluorescence signal increase for each amplification group. We found no significant difference in fluorescence signal between all amplification times for gRNA-S3 (15 vs 30 m: $p = 0.5576$, 15 vs 45 m: $p = 0.9935$, 30 vs 45 m: $p = 0.2735$); however, for gRNA-N1, fluorescence signal in the 15 min

https://doi.org/10.1021/acssensors.1c01088
ACS Sens. XXXX, XXX, XXX−XXX

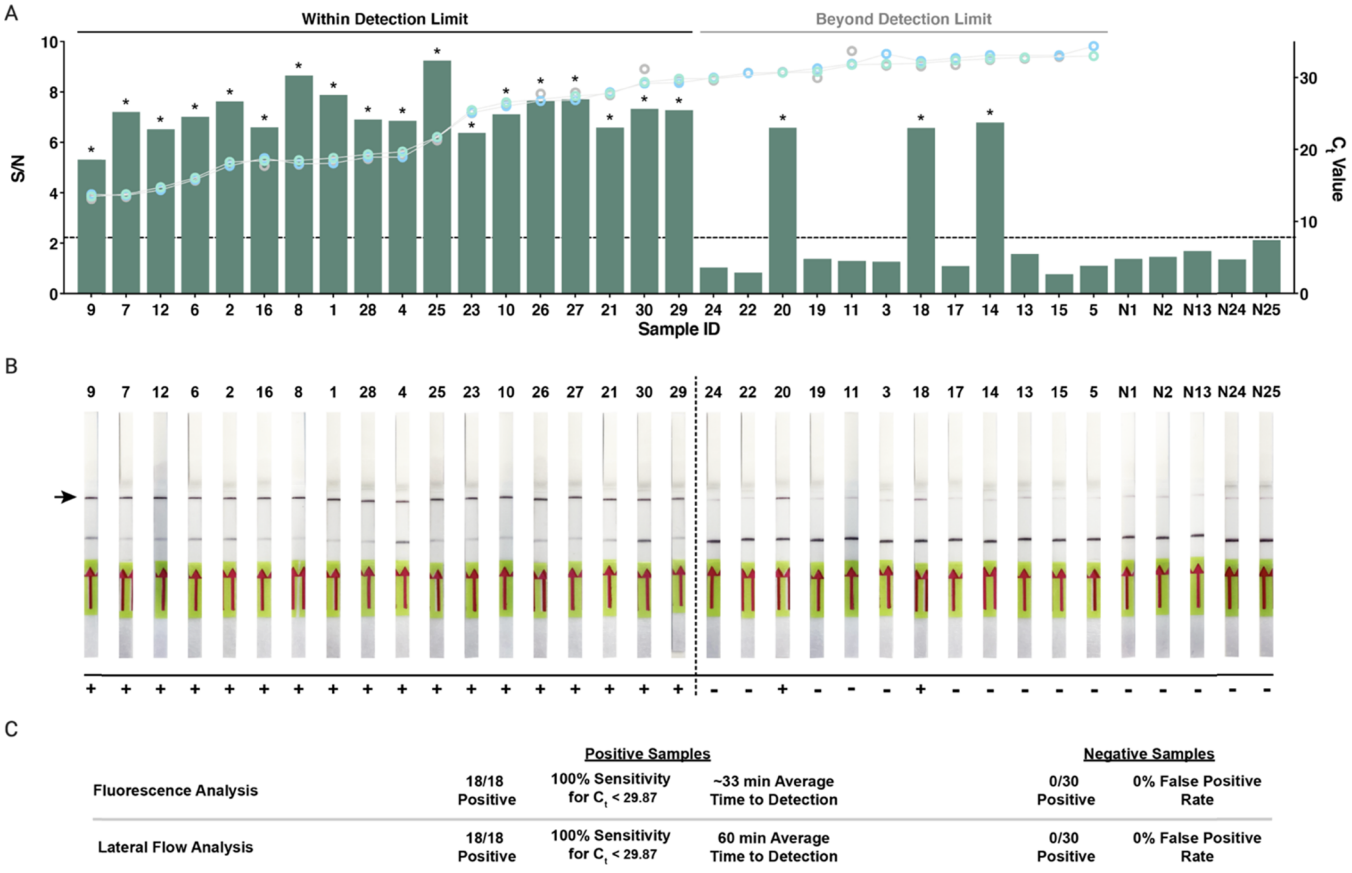

Figure 3. SENSR detection of positive SARS-CoV-2 validated patient samples. (A) SENSR fluorescence analysis of RT-qPCR validated patient samples using gRNA-S3 for detection. Signal-to-noise (S/N) ratio of 30 positive and five negative samples are shown. Positive samples are listed in order from lowest to highest C_t value for S-gene. Open circles represent C_t value of S- (light green), N- (blue), and Orf1ab (gray). The five negative samples are negative samples with the highest calculated S/N ratio among all negative samples analyzed. The dashed line represents the S/N threshold = 2.22. Asterisks represent a S/N > 2.22. (B) Lateral flow-based detection of the 30 positive and five negative samples. The top band (arrow) represents the test band and, the bottom, the control band. An increase in the saturation of the top band indicates a positive detection of SARS-CoV-2 in the sample. The vertical dashed line indicates the detection limit. The result of detection is indicated below each test strip. (C) Summary of fluorescence and lateral flow detection results for the RT-qPCR validated positive and negative patient samples.

amplification group was significantly lower than 30 and 45 min amplification times (15 vs 30 m and 15 vs 45 m: $p < 0.0001$) (Figure S8C,D). We therefore selected 30 min amplification as the standard time of amplification for future fluorescence experiments.

Fluorescence Limit of Detection. Following optimization of SENSR fluorescence reaction parameters, we moved on to determine the limit of detection (LoD) for gRNA-S3 and gRNA-N1 via serial dilution of the synthetic RNA templates from 10 000 to 0 copy/μL added directly into RT-RPA reactions. For both gRNA-S3 and gRNA-N1, we observed a significant increase in fluorescence signal above the noise for 10 000, 1000, and 100 copies compared to the NTC (Figure 2A,B). Interestingly, we also observed significantly higher fluorescence at 10 copies for gRNA-S3 (Figure 2A); however, this signal increase was not comparable to the increase observed in higher copy groups (Dunnett's multiple comparisons test; 10 000, 1000, 100 copies vs 10: $p < 0.0001$). We therefore determined the LOD for synthetic RNA to be 100 copy/μL for both gRNA-S3 and gRNA-N1, indicating that SENSR exhibits attomolar analytical sensitivity comparable to other CRISPRDx systems.[11,13] These results demonstrate that CasRx can robustly detect and report the presence of synthetic SARS-CoV-2 RNA via fluorescence readout.

Lateral Flow Assay Development. Collateral cleavage by CasRx can additionally be exploited to detect SARS-CoV-2 RNA by LF readout, which facilitates detection by simple paper test strips and eliminates the need for expensive laboratory equipment (Figures 1A and S3). Similar to previously developed assays,[12,33] we generated a 6 nt ssRNA probe modified with 5′ 6-FAM and 3′ biotin (Bio) compatible with Millenia HybriDetect LF strips (Table S4). In brief, collateral cleavage results in separation of 6-FAM from biotin, detectable following capillary action down a paper dipstick imprinted with streptavidin and anti-FAM secondary antibodies at distant ends (Figure 1A). An increase in the saturation of the upper band, or lack thereof, indicates a positive or negative result, respectively (summarized in Figures 1A and S3).

LF protocols only allow one-time point for assessing detection, and we therefore optimized the SENSR protocol by varying the amplification and cleavage times for our LF assay. We amplified the synthetic SARS-CoV-2 template for 15, 30, or 45 min and then proceeded to incubate the CCR for 15, 30, or 45 min. We observed cleavage of the LF probe at all amplification times in all cleavage times tested with clear evidence that extended cleavage time enhances detection, while extended amplification time does not have a dramatic effect on detection (Figure S9). In an effort to keep the total processing

https://doi.org/10.1021/acssensors.1c01088
ACS Sens. XXXX, XXX, XXX−XXX

time within 1 h, we chose 30 min amplification and 30 min cleavage for our standard protocol. This decision was driven by fluorescence evidence, suggesting that gRNA-N1 requires at least 30 min of amplification to increase the rate of probe cleavage for sufficient detection at lower copy numbers (Figure S8B).

Using this optimized protocol, we then determined the LoD of SENSR in a LF assay format by performing a serial dilution of the synthetic RNA templates from 10 000 to 0 copy/μL added directly into RT-RPA reactions. We determined the LoD for each gRNA detecting synthetic RNA to be 100 copy/μL, where gRNA-S3 exhibited significantly more probe cleavage compared to gRNA-N1 (Figure 2C,D, Supporting Information Video 1). These results confirm that SENSR, like other CRISPRDx systems, can be adapted for readout by LF, indicating the potential for future point-of-care applications.

SENSR Detection of SARS-CoV-2 from Patient Isolates. Previously, we analyzed a set of RT-qPCR-verified patient samples using a preliminary protocol for SENSR and targeting a different segment of the N-gene (Tables S4, S6, and S7). We observed only moderate detection of patient samples, with 92% of samples detected for $C_t \leq 20$. The highest C_t value detected was 27.5, and we observed a 23 and 28% false-negative rate for $C_t \leq 27.5$ for fluorescence and lateral flow, respectively (Figure S10). Furthermore, this version of SENSR took nearly 2 h to obtain results from both readouts. Therefore, we further optimized SENSR and improved the sensitivity and time to detection, as previously described (Figures S7−S9).

Following optimization, we set out to determine the ability of SENSR to detect SARS-CoV-2 from clinically verified patient samples. Samples were analyzed by RT-qPCR, targeting the N-, S-, and Orf1ab-genes (Table S7), and accordingly, we selected gRNA-S3 and gRNA-N1 to directly compare detection by SENSR to RT-qPCR. We performed fluorescence and LF analysis on 60 total samples: 30 positive ($n = 30$) (C_t range: 13−34) and 30 negative samples. The C_t values of the positive patient samples were distributed as follows: 13.3% (4) <17*, 23.3% (7) between 17 and 22, 16.7% (5) between 22* and 29*, and 46.7% (14) between 29 and 34.

From the patient samples tested, we observed considerably different results from each gRNA applied. gRNA-N1 performed less effectively than gRNA-S3, detecting only 17/30 positive samples by fluorescence and 16/30 samples by LF (Figure S11, Table S7), whereas gRNA-S3 detected 21/30 positive samples by fluorescence, 20/30 samples by LF (Figure 3, Table S7). gRNA-S3 exhibited a 0% false-positive rate in both readouts, while gRNA-N1 resulted in a 3.3% false-positive rate by fluorescence readout (Figures 3, S11, and S12). Furthermore, each gRNA resulted in different detection limits based on copy number values extrapolated from the RT-qPCR standard curve (Figure S13). To elaborate, gRNA-S3 detected SARS-CoV-2 in 100% of samples (18/18) by both readouts for samples with a $C_t \leq 29.83$ (45 copy/μL), whereas gRNA-N1 detected vRNA in 94% (16/17) and 88% (15/17) of samples for fluorescence and LF, respectively, for samples with $C_t \leq 29.28$ (87 copy/μL) (Figures 3, S11A, and S13, Table S7).

LF-based detection methods are limited to one detection point; however, fluorescence data are acquired multiple times during incubation of the CCR. Therefore, we further evaluated the fluorescence data to find the time each sample crossed the signal-to-noise (S/N) threshold, thus determining a positive result. We found gRNA-S3 detected SARS-CoV-2 in patient samples between 30.58 and 40.98 min total reaction time (RT-RPA + CCR) and on average detected vRNA within 33.05 min. gRNA-N1 detected vRNA in patient samples between 30.76 and 59.86 min total reaction time 34.27 min on average (Table S8). Taken together, these results demonstrate that SENSR rapidly detects SARS-CoV-2 from patient isolates and exhibits sensitivity comparable to previously established CRISPRDx systems.[20]

DISCUSSION

Complementing the rapidly expanding CRISPRDx toolkit, here we outline the use of CasRx to detect SARS-CoV-2. The development of SENSR establishes proof-of-principle that Cas13d ribonucleases can be adapted for nucleic acid diagnostics. Identifying targets conserved and specific to SARS-CoV-2, we applied SENSR and demonstrated detection with attomolar sensitivity by both fluorescence and lateral flow readouts comparable to previously developed systems.[20,24,39] Furthermore, we determined the CasRx collateral cleavage sequence preference for uracil stretches over all other di-nucleotide combinations, demonstrating promise for multiplexing applications.[12,33] Together, these results demonstrate and provide evidence that SENSR can be adapted and further optimized for the detection of a multitude of pathogens (Figure S14).

Comparatively, SENSR may present a worthy advancement for the CRISPRDx toolkit due to the fundamental properties of Cas13d effectors. Similar to LwaCas13a used in SHERLOCK systems, Cas13d effectors are more flexible than most Cas enzymes as they lack a protospacer flanking sequence (PFS) requirement,[17,30,32] permitting targeting of any sequence. Moreso, we demonstrate SENSR exhibits comparable sensitivity to SHERLOCK,[20] suggesting CasRx as a viable alternative to LwaCas13a for nucleic acid detection. CasRx also presents great potential for multiplexing applications with other Cas13 effectors due to the uracil-specific collateral cleavage activity.[12] Due to the stringent criteria required for diagnostics, further optimization in advance of deployment is necessary. However, the flexible targeting, multiplexing capabilities, and sensitivity of SENSR present a potentially viable technology for disease diagnosis and establish an alternative Cas effector subtype for nucleic acid detection.

SENSR presents great promise for future applications; however, improvements to the system may be necessary. For instance, RT-RPA is less sensitive than RT-LAMP,[40] and therefore, alternative isothermal amplification methods could further improve sensitivity. Although RT-LAMP is likely to improve sensitivity, the requirement of two separate reactions remains problematic, as this increases the likelihood of contamination due to sample transfers.[41] Direct detection of RNA with CasRx could reduce the need for multiple transfers, as has been demonstrated with LbuCas13a.[42] However, CasRx direct detection only demonstrated picomolar sensitivity (Figure S15), whereas SENSR exhibits attomolar sensitivity—a significant increase in sensitivity largely due to the preamplification via RT-RPA. Furthermore, considerable variation in sensitivities have been reported for different Cas13 enzymes, and detection accuracy of LbuCas13a at 100 copy/μL drops 20% using direct detection in a POC format.[42] Finally, differences in gRNA sensitivities were observed in our analysis of infected patient samples, and thus improvements to gRNA screening and selection could expedite the response time to future disease outbreaks.[43]

https://doi.org/10.1021/acssensors.1c01088
ACS Sens. XXXX, XXX, XXX−XXX

Optimizing workflow, deployment, and distribution while taking steps to reduce the risk of contamination is imperative to develop SENSR to its full potential. We demonstrate that detection with CasRx is a viable alternative for nucleic acid detection and could be further improved to become a powerful molecular diagnostic with numerous applications. Establishing these tools and frameworks now could expedite response times and help prevent future outbreaks, avoiding the economic and health consequences that have resulted from poor preparedness to the current pandemic.

MATERIALS AND METHODS

***In Vitro* gRNA Cleavage Assays.** Preliminary *in vitro* cleavage assays were prepared with RNA templates for S-gene (1000 ng) or N-gene (1200 ng), followed by the addition of CasRx (110.8 ng) and 10 ng of each gRNA in a 2:1 molar ratio. Reactions were prepared in 20 mM HEPES pH 7.2 and 9 mM $MgCl_2$, incubated at 37 °C for 1 h, and then denatured at 85 °C for 10 min in 2× RNA loading dye (New England Biolabs, #B0363) and loaded on 2% TBE agarose gel stained with SYBR gold nucleic acid stain (Invitrogen #S11494).

RT-RPA Amplification of Viral Genomic Sequences. RT-RPA primers were designed to amplify 30 bp gRNA spacer regions flanked by 30 bp priming regions from the synthetic vRNA template while also incorporating a T7 promoter sequence into the 5′ end of the dsDNA gene fragment with +2 G's, thus increasing the transcription efficiency (Figure 1B).[44] RT-RPA was performed at 42 °C for 30 min by combining M-MuLV-RT (NEB #M0253L) with TwistAmp Basic (TwistDx #TABAS03KIT). All RT-RPA primer sequences can be found in Table S1. Final conditions for optimized (28.5% sample input) RT-RPA protocol in 10 μL reaction: 5.9 μL rehydration buffer, 0.35 μL primer mix (10 μM each), 0.4 μL RT (200 U/μL), 0.5 μL MgOAc (280 mM), and 2.85 μL vRNA.

Fluorescence-Based Detection of SARS-CoV-2. We developed an IVT-coupled cleavage assay with a fluorescence readout using 6-carboxyfluorescein (6-FAM) as our fluorescent molecule. We developed a 6 nt poly-U probe conjugated to a 5′ 6-FAM and a 3′ IABlkFQ (FRU, Table S4) and custom-ordered from IDT. Probes with variable di-nucleotide repeat sequences were ordered from IDT and can be found in Table S4. Direct detection experiments were performed in 20 μL reactions as follows: 13.32 μL water, 0.4 μL HEPES pH 7.2 (1 M), 0.24 μL $MgCl_2$ (1 M), 2 μL CasRx (55.4 ng/μL), 1 μL RNase inhibitor (40 U/μL), 1 μL gRNA (10 ng/μL), and 1 μL FRU probe (2 μM). Optimized fluorescence protocol (10 μL): 2.82 μL water, 0.4 μL HEPES pH 7.2 (1 M), 0.18 μL $MgCl_2$ (1 M), 1 μL rNTPs (25 mM each), 2 μL CasRx (55.4 ng/μL), 1 μL RNase inhibitor (40 U/μL), 0.6 μL T7 Polymerase (50 U/μL), 1 μL gRNA (10 ng/μL), and 1 μL FRU probe (2 μM). This was followed by the addition of 10 μL (100% RT-RPA reaction vol) of the RT-RPA preamplification reaction (described above), which initiates detection following incubation at 37 °C for 60 min. Experiments were immediately run on a LightCycler 96 (Roche #05815916001) at 37 °C. Acquisition protocol: 5 s acquisition followed by 5 s incubation for the first 15 min, followed by 5 s acquisition and 55 s incubation for up to 45 min. Fluorescence readouts were analyzed by normalization to NTC at each respective time point or through background-subtracted fluorescence by subtracting the initial fluorescence value from the final value.

Lateral Flow Detection of SARS-CoV-2. For lateral flow-based detection, we modified the HybriDetect system to detect the presence of SARS-CoV-2 sequences using SENSR.[24] In brief, we designed a ssRNA probe composed of a 6 nt poly-U probe conjugated on opposite ends with a 5′ 6-FAM and a 3′ biotin, which was custom-ordered from IDT (LFRU, Table S4). Following incubation of 2.82 μL water, 0.4 μL HEPES pH 7.2 (1 M), 0.18 μL $MgCl_2$ (1 M), 2 μL CasRx (55.4 ng/μL), 1 μL gRNA (10 ng/μL), 10 μL RT-RPA reaction mix, 0.6 μL T7 RNA polymerase (50 U/μL), 1 μL rNTPs (25 mM each), and 1 μL LFRU probe (20 μM), at 37 °C for 30 min. Typically, 80 μL of HybriDetect assay buffer was added to each reaction. Next, the lateral flow dipstick was placed into the reaction and allowed to flow upward by capillary action for a maximum of 3 min. The presence or absence of upper or lower bands was analyzed to detect the evidence of SARS-CoV-2 by collateral cleavage. The presence of a solitary upper band or both an upper and lower band was interpreted as a positive result; a solitary lower band with a faint upper band was interpreted as a negative result.

LoD Analysis. For SENSR LoD analysis against synthetic RNA, synthetic templates were serially diluted on a logarithmic scale. Template stock concentrations were analyzed via a NanoDrop prior to dilutions. Dilution scales were calculated using NEBioCalculator for each respective template. For fluorescence analysis, the LoD was determined by statistical significance of the lowest copy number experimental group compared to the NTC. For lateral flow analysis, the LoD was determined by noticeable saturation of the upper test band compared to the NTC.

LoD for RT-qPCR was performed by spiking viral particles into verified SARS-CoV-2 negative samples contained in viral transport media (VTM) at specified copy numbers. Typically, 2 μL of the extracted sample was run for the assay; therefore, all copy/μL values must be multiplied by 2 (Figure S13A).

SENSR detection limit in patient samples was calculated by performing nonlinear regression analysis and fitting a semi-log function ($y = b + m$*log(x), where b is the y-intercept and m is the slope) to the data where x values are treated as log and y values as linear (Figure S13A). We then solved for x to generate a function for calculating the copy/μL based on C_t value ($x = 10^{(y-b)/m}$). Copy/μL values were then calculated by entering the C_t value of each sample for y and multiplying x by 2 (for each μL added).

SENSR Detection of Patient Samples. Fluorescence and LF assays were run against SARS-CoV-2 positive ($N = 30$) and negative ($N = 30$) samples. Samples were amplified for 30 min RT-RPA reaction at 28.5% v/v. Then, 10 μL of RT-RPA reaction was incubated in a CCR reaction, as previously described. Fluorescence data for analysis were acquired on LightCycler 96 (Roche #05815916001), following the protocol previously described. Data were processed by generating background-subtracted fluorescence for each replicate by subtracting the final (30 min) fluorescence value from the initial (0 min) fluorescence value. Noise was set as the average of the four NTC background-subtracted values. S/N was then calculated by dividing the background-subtracted value for each sample by the noise. To account for 99.9% of expected negative sample S/N measurements, the S/N threshold was set at $\mu + 3.5\sigma$ of the negative samples. Samples were determined to be positive if S/N > 2.22 for gRNA-S3 and positive if S/N > 3.51 for gRNA-N1. Time to detection was calculated by calculating S/N at each time point, where N is equal to the average of NTC after 30 min.

Lateral flow analysis was run in parallel to fluorescence analysis. The samples were amplified via RT-RPA for 30 min at 28.5% v/v. Then, 10 μL of RT-RPA was transferred to the cleavage reaction with LFRU and incubated at 37 °C for 30 min. LF analysis was then performed with 3 min incubation of strips. Images were taken using an iPhone 12 mini. Positives and negatives were determined in comparison to the NTC samples and using a positive control (synthetic template) as a standard.

ASSOCIATED CONTENT

Supporting Information

The Supporting Information is available free of charge at https://pubs.acs.org/doi/10.1021/acssensors.1c01088.

Tables with sequence information and reaction conditions (XLSX)

All possible 30 nt sequences were extracted from 433 published SARS-CoV-2 genomes using a Perl script (File S1) (TXT)

Movie depicting the limit of detection experiment using the lateral flow readout (MOV)

Figures for supportive data and methods descriptions (PDF)

https://doi.org/10.1021/acssensors.1c01088
ACS Sens. XXXX, XXX, XXX−XXX

AUTHOR INFORMATION

Corresponding Author

Omar S. Akbari − *Division of Biological Sciences, Section of Cell and Developmental Biology, University of California San Diego, La Jolla, California 92093, United States;* orcid.org/0000-0002-6853-9884; Email: oakbari@ucsd.edu

Authors

Daniel J. Brogan − *Division of Biological Sciences, Section of Cell and Developmental Biology, University of California San Diego, La Jolla, California 92093, United States;* orcid.org/0000-0001-6582-8966

Duverney Chaverra-Rodriguez − *Division of Biological Sciences, Section of Cell and Developmental Biology, University of California San Diego, La Jolla, California 92093, United States*

Calvin P. Lin − *Department of Chemistry and Biochemistry, University of California San Diego, La Jolla, California 92092, United States*

Andrea L. Smidler − *Division of Biological Sciences, Section of Cell and Developmental Biology, University of California San Diego, La Jolla, California 92093, United States*

Ting Yang − *Division of Biological Sciences, Section of Cell and Developmental Biology, University of California San Diego, La Jolla, California 92093, United States*

Lenissa M. Alcantara − *Division of Biological Sciences, Section of Cell and Developmental Biology, University of California San Diego, La Jolla, California 92093, United States*

Igor Antoshechkin − *Division of Biology and Biological Engineering, California Institute of Technology, Pasadena, California 91125, United States*

Junru Liu − *Division of Biological Sciences, Section of Cell and Developmental Biology, University of California San Diego, La Jolla, California 92093, United States*

Robyn R. Raban − *Division of Biological Sciences, Section of Cell and Developmental Biology, University of California San Diego, La Jolla, California 92093, United States*

Pedro Belda-Ferre − *Department of Pediatrics, University of California San Diego, La Jolla, California 92161, United States*

Rob Knight − *Department of Pediatrics, University of California San Diego, La Jolla, California 92161, United States; Center for Microbiome Innovation, Department of Computer Science and Engineering, and Department of Bioengineering, University of California San Diego, La Jolla, California 92093, United States*

Elizabeth A. Komives − *Department of Chemistry and Biochemistry, University of California San Diego, La Jolla, California 92092, United States;* orcid.org/0000-0001-5264-3866

Complete contact information is available at: https://pubs.acs.org/10.1021/acssensors.1c01088

Author Contributions

○D.J.B., D.C.-R., and C.P.L. are equal first author contributions.

Author Contributions

▽A.L.S. and T.Y. are equal second author contributions. O.S.A. conceptualized the study. D.J.B., D.C.-R., C.P.L., J.L., L.M.A., T.Y., I.A., and P.B.-F., performed, designed, and analyzed various molecular, bioinformatic, and protein biochemistry. A.L.S., R.R.R., R.K., and E.A.K. contributed to analyzing and designing experiments. All authors contributed to writing, analyzing the data, and approving the final manuscript.

Notes

The authors declare the following competing financial interest(s): O.S.A. has a patent pending on this technology. All other authors declare no significant competing financial, professional, or personal interests that might have influenced the performance or presentation of the work described.

Bioinformatic scripts can be found in File S1. A limited quantity of CasRx enzyme will be made available upon request.

ACKNOWLEDGMENTS

We thank the SEARCH (San Diego Epidemiology and Research for COVID-19 Health) Alliance for providing clinical samples. This work was supported in part by UCSD Seed Funds for Emergent COVID-19 Related Research, a Directors New Innovator award from NIH/NIAID (DP2 AI152071-01), NIH/NIAID R21 (1R21AI149161), and a DARPA Safe Genes Program Grant (HR0011-17-2-0047) awarded to O.S.A., and a Director's Pioneer Award from NCCIH (DP1 AT010885) to R.K., and the Molecular Biophysics Training Grant from NIH (T32 GM00832) to C.P.L., and the UCSD Return to Learn program via the EXCITE (EXpedited COVID-19 IdenTification Environment) lab. The views, opinions, and/or findings expressed should not be interpreted as representing the official views or policies of the Department of Defense or the U.S. Government. C.P.L. was supported by the Molecular Biophysics Training Grant, NIH Grant T32 GM00832.

REFERENCES

(1) Zhu, N.; Zhang, D.; Wang, W.; Li, X.; Yang, B.; Song, J.; Zhao, X.; Huang, B.; Shi, W.; Lu, R.; Niu, P.; Zhan, F.; Ma, X.; Wang, D.; Xu, W.; Wu, G.; Gao, G. F.; Tan, W.; China Novel Coronavirus Investigating and Research Team. A Novel Coronavirus from Patients with Pneumonia in China, 2019. *N. Engl. J. Med.* **2020**, *382*, 727−733.

(2) Mallapaty, S. Animal Source of the Coronavirus Continues to Elude Scientists. *Nature* **2020**. DOI: 10.1038/d41586-020-01449-8.

(3) Andersen, K. G.; Rambaut, A.; Lipkin, W. I.; Holmes, E. C.; Garry, R. F. The Proximal Origin of SARS-CoV-2. *Nat. Med.* **2020**, *26*, 450−452.

(4) Wang, C.; Horby, P. W.; Hayden, F. G.; Gao, G. F. A Novel Coronavirus Outbreak of Global Health Concern. *Lancet* **2020**, *395*, 470−473.

(5) WHO *Coronavirus Disease 2019 (COVID-19) Situation Report - 93*; WHO, 2020.

(6) Vogels, C. B. F.; Brito, A. F.; Wyllie, A. L.; Fauver, J. R.; Ott, I. M.; Kalinich, C. C.; Petrone, M. E.; Casanovas-Massana, A.; Catherine Muenker, M.; Moore, A. J.; Klein, J.; Lu, P.; Lu-Culligan, A.; Jiang, X.; Kim, D. J.; Kudo, E.; Mao, T.; Moriyama, M.; Oh, J. E.; Park, A.; Silva, J.; Song, E.; Takahashi, T.; Taura, M.; Tokuyama, M.; Venkataraman, A.; Weizman, O.-E.; Wong, P.; Yang, Y.; Cheemarla, N. R.; White, E. B.; Lapidus, S.; Earnest, R.; Geng, B.; Vijayakumar, P.; Odio, C.; Fournier, J.; Bermejo, S.; Farhadian, S.; Dela Cruz, C. S.; Iwasaki, A.; Ko, A. I.; Landry, M. L.; Foxman, E. F.; Grubaugh, N. D. Analytical Sensitivity and Efficiency Comparisons of SARS-CoV-2 RT-qPCR Primer-Probe Sets. *Nat. Microbiol.* **2020**, *5*, 1299−1305.

(7) Rezaei, M.; Razavi Bazaz, S.; Zhand, S.; Sayyadi, N.; Jin, D.; Stewart, M. P.; Ebrahimi Warkiani, M. Point of Care Diagnostics in the Age of COVID-19. *Diagnostics* **2020**, *11*, No. 9.

(8) Jinek, M.; Chylinski, K.; Fonfara, I.; Hauer, M.; Doudna, J. A.; Charpentier, E. A Programmable Dual-RNA-Guided DNA Endonuclease in Adaptive Bacterial Immunity. *Science* **2012**, *337*, 816−821.

(9) Abudayyeh, O. O.; Gootenberg, J. S.; Konermann, S.; Joung, J.; Slaymaker, I. M.; Cox, D. B. T.; Shmakov, S.; Makarova, K. S.; Semenova, E.; Minakhin, L.; Severinov, K.; Regev, A.; Lander, E. S.; Koonin, E. V.; Zhang, F. C2c2 Is a Single-Component Programmable

RNA-Guided RNA-Targeting CRISPR Effector. *Science* **2016**, *353*, No. aaf5573.
(10) Zetsche, B.; Gootenberg, J. S.; Abudayyeh, O. O.; Slaymaker, I. M.; Makarova, K. S.; Essletzbichler, P.; Volz, S. E.; Joung, J.; van der Oost, J.; Regev, A.; Koonin, E. V.; Zhang, F. Cpf1 Is a Single RNA-Guided Endonuclease of a Class 2 CRISPR-Cas System. *Cell* **2015**, *163*, 759−771.
(11) Gootenberg, J. S.; Abudayyeh, O. O.; Lee, J. W.; Essletzbichler, P.; Dy, A. J.; Joung, J.; Verdine, V.; Donghia, N.; Daringer, N. M.; Freije, C. A.; Myhrvold, C.; Bhattacharyya, R. P.; Livny, J.; Regev, A.; Koonin, E. V.; Hung, D. T.; Sabeti, P. C.; Collins, J. J.; Zhang, F. Nucleic Acid Detection with CRISPR-Cas13a/C2c2. *Science* **2017**, 438−442.
(12) Gootenberg, J. S.; Abudayyeh, O. O.; Kellner, M. J.; Joung, J.; Collins, J. J.; Zhang, F. Multiplexed and Portable Nucleic Acid Detection Platform with Cas13, Cas12a, and Csm6. *Science* **2018**, *360*, 439−444.
(13) Chen, J. S.; Ma, E.; Harrington, L. B.; Da Costa, M.; Tian, X.; Palefsky, J. M.; Doudna, J. A. CRISPR-Cas12a Target Binding Unleashes Indiscriminate Single-Stranded DNase Activity. *Science* **2018**, *360*, 436−439.
(14) Li, S.-Y.; Cheng, Q.-X.; Wang, J.-M.; Li, X.-Y.; Zhang, Z.-L.; Gao, S.; Cao, R.-B.; Zhao, G.-P.; Wang, J. CRISPR-Cas12a-Assisted Nucleic Acid Detection. *Cell Discovery* **2018**, *4*, No. 20.
(15) Azhar, M.; Phutela, R.; Kumar, M.; Ansari, A. H.; Rauthan, R.; Gulati, S.; Sharma, N.; Sinha, D.; Sharma, S.; Singh, S.; Acharya, S.; Sarkar, S.; Paul, D.; Kathpalia, P.; Aich, M.; Sehgal, P.; Ranjan, G.; Bhoyar, R. C.; Indian CoV2 Genomics & Genetic Epidemiology (IndiCovGEN) Consortium; Singhal, K.; Lad, H.; Patra, P. K.; Makharia, G.; Chandak, G. R.; Pesala, B.; Chakraborty, D.; Maiti, S. Rapid and Accurate Nucleobase Detection Using FnCas9 and Its Application in COVID-19 Diagnosis. *Biosens. Bioelectron.* **2021**, *183*, No. 113207.
(16) Harrington, L. B.; Burstein, D.; Chen, J. S.; Paez-Espino, D.; Ma, E.; Witte, I. P.; Cofsky, J. C.; Kyrpides, N. C.; Banfield, J. F.; Doudna, J. A. Programmed DNA Destruction by Miniature CRISPR-Cas14 Enzymes. *Science* **2018**, *362*, 839−842.
(17) Freije, C. A.; Myhrvold, C.; Boehm, C. K.; Lin, A. E.; Welch, N. L.; Carter, A.; Metsky, H. C.; Luo, C. Y.; Abudayyeh, O. O.; Gootenberg, J. S.; Yozwiak, N. L.; Zhang, F.; Sabeti, P. C. Programmable Inhibition and Detection of RNA Viruses Using Cas13. *Mol. Cell* **2019**, *76*, 826−837.e11.
(18) Mukama, O.; Wu, J.; Li, Z.; Liang, Q.; Yi, Z.; Lu, X.; Liu, Y.; Liu, Y.; Hussain, M.; Makafe, G. G.; Liu, J.; Xu, N.; Zeng, L. An Ultrasensitive and Specific Point-of-Care CRISPR/Cas12 Based Lateral Flow Biosensor for the Rapid Detection of Nucleic Acids. *Biosens. Bioelectron.* **2020**, No. 112143.
(19) Hajian, R.; Balderston, S.; Tran, T.; deBoer, T.; Etienne, J.; Sandhu, M.; Wauford, N. A.; Chung, J.-Y.; Nokes, J.; Athaiya, M.; Paredes, J.; Peytavi, R.; Goldsmith, B.; Murthy, N.; Conboy, I. M.; Aran, K. Detection of Unamplified Target Genes via CRISPR-Cas9 Immobilized on a Graphene Field-Effect Transistor. *Nat. Biomed. Eng.* **2019**, *3*, 427−437.
(20) Patchsung, M.; Jantarug, K.; Pattama, A.; Aphicho, K.; Suraritdechachai, S.; Meesawat, P.; Sappakhaw, K.; Leelahakorn, N.; Ruenkam, T.; Wongsatit, T.; Athipanyasilp, N.; Eiamthong, B.; Lakkanasirorat, B.; Phoodokmai, T.; Niljianskul, N.; Pakotiprapha, D.; Chanarat, S.; Homchan, A.; Tinikul, R.; Kamutira, P.; Phiwkaow, K.; Soithongcharoen, S.; Kantiwiriyawanitch, C.; Pongsupasa, V.; Trisrivirat, D.; Jaroensuk, J.; Wongnate, T.; Maenpuen, S.; Chaiyen, P.; Kamnerdnakta, S.; Swangsri, J.; Chuthapisith, S.; Sirivatanauksorn, Y.; Chaimayo, C.; Sutthent, R.; Kantakamalakul, W.; Joung, J.; Ladha, A.; Jin, X.; Gootenberg, J. S.; Abudayyeh, O. O.; Zhang, F.; Horthongkham, N.; Uttamapinant, C. Clinical Validation of a Cas13-Based Assay for the Detection of SARS-CoV-2 RNA. *Nat. Biomed. Eng.* **2020**, 1140−1149.
(21) Joung, J.; Ladha, A.; Saito, M.; Kim, N.-G.; Woolley, A. E.; Segel, M.; Barretto, R. P. J.; Ranu, A.; Macrae, R. K.; Faure, G.; Ioannidi, E. I.; Krajeski, R. N.; Bruneau, R.; Huang, M.-L. W.; Yu, X. G.; Li, J. Z.; Walker, B. D.; Hung, D. T.; Greninger, A. L.; Jerome, K. R.; Gootenberg, J. S.; Abudayyeh, O. O.; Zhang, F. Detection of SARS-CoV-2 with SHERLOCK One-Pot Testing. *N. Engl. J. Med.* **2020**, 1492−1494.
(22) Ding, X.; Yin, K.; Li, Z.; Lalla, R. V.; Ballesteros, E.; Sfeir, M. M.; Liu, C. Ultrasensitive and Visual Detection of SARS-CoV-2 Using All-in-One Dual CRISPR-Cas12a Assay. *Nat. Commun.* **2020**, *11*, No. 4711.
(23) Broughton, J. P.; Deng, X.; Yu, G.; Fasching, C. L.; Servellita, V.; Singh, J.; Miao, X.; Streithorst, J. A.; Granados, A.; Sotomayor-Gonzalez, A.; Zorn, K.; Gopez, A.; Hsu, E.; Gu, W.; Miller, S.; Pan, C.-Y.; Guevara, H.; Wadford, D. A.; Chen, J. S.; Chiu, C. Y. CRISPR-Cas12-Based Detection of SARS-CoV-2. *Nat. Biotechnol.* **2020**, 870−874.
(24) Zhang, F.; Abudayyeh, O. O.; Jonathan, S. G. A Protocol for Detection of COVID-19 Using CRISPR Diagnostics. 2020 https://www.broadinstitute.org/files/publications/special/COVID-19%20detection%20(updated).pdf (accessed 2021-10-28).
(25) Abbott, T. R.; Dhamdhere, G.; Liu, Y.; Lin, X.; Goudy, L.; Zeng, L.; Chemparathy, A.; Chmura, S.; Heaton, N. S.; Debs, R.; Pande, T.; Endy, D.; La Russa, M. F.; Lewis, D. B.; Qi, L. S. Development of CRISPR as an Antiviral Strategy to Combat SARS-CoV-2 and Influenza. *Cell* **2020**, *181*, 865−876.e12.
(26) Ackerman, C. M.; Myhrvold, C.; Thakku, S. G.; Freije, C. A.; Metsky, H. C.; Yang, D. K.; Ye, S. H.; Boehm, C. K.; Kosoko-Thoroddsen, T.-S. F.; Kehe, J.; Nguyen, T. G.; Carter, A.; Kulesa, A.; Barnes, J. R.; Dugan, V. G.; Hung, D. T.; Blainey, P. C.; Sabeti, P. C. Massively Multiplexed Nucleic Acid Detection Using Cas13. *Nature* **2020**, 277−282.
(27) Rauch, J. N.; Valois, E.; Solley, S. C.; Braig, F.; Lach, R. S.; Audouard, M.; Ponce-Rojas, J. C.; Costello, M. S.; Baxter, N. J.; Kosik, K. S.; Arias, C.; Acosta-Alvear, D.; Wilson, M. Z. A Scalable, Easy-to-Deploy Protocol for Cas13-Based Detection of SARS-CoV-2 Genetic Material. *J. Clin. Microbiol.* **2021**, *59*, No. e02402-20.
(28) Metsky, H. C.; Freije, C. A.; Kosoko-Thoroddsen, T.-S. F.; Sabeti, P. C.; Myhrvold, C. CRISPR-Based Surveillance for COVID-19 Using Genomically-Comprehensive Machine Learning Design. *bioRxiv* 2020, 967026. DOI: 10.1101/2020.02.26.967026.
(29) Lucia, C.; Federico, P.-B.; Alejandra, G. C. An Ultrasensitive, Rapid, and Portable Coronavirus SARS-CoV-2 Sequence Detection Method Based on CRISPR-Cas12. *bioRxiv* 2020, 971127. DOI: 10.1101/2020.02.29.971127.
(30) Konermann, S.; Lotfy, P.; Brideau, N. J.; Oki, J.; Shokhirev, M. N.; Hsu, P. D. Transcriptome Engineering with RNA-Targeting Type VI-D CRISPR Effectors. *Cell* **2018**, *173*, 665−676.e14.
(31) Buchman, A. B.; Brogan, D. J.; Sun, R.; Yang, T.; Hsu, P. D.; Akbari, O. S. Programmable RNA Targeting Using CasRx in Flies. *CRISPR J.* **2020**, *3*, 164−176.
(32) Yan, W. X.; Chong, S.; Zhang, H.; Makarova, K. S.; Koonin, E. V.; Cheng, D. R.; Scott, D. A. Cas13d Is a Compact RNA-Targeting Type VI CRISPR Effector Positively Modulated by a WYL-Domain-Containing Accessory Protein. *Mol. Cell* **2018**, *70*, 327−339.e5.
(33) Kellner, M. J.; Koob, J. G.; Gootenberg, J. S.; Abudayyeh, O. O.; Zhang, F. SHERLOCK: Nucleic Acid Detection with CRISPR Nucleases. *Nat. Protoc.* **2019**, *14*, 2986−3012.
(34) Sun, R.; Brogan, D.; Buchman, A.; Yang, T.; Akbari, O. S. Ubiquitous and Tissue-Specific RNA Targeting in Drosophila Melanogaster Using CRISPR/CasRx. *J. Visualized Exp.* **2021**, No. e62154.
(35) Kushawah, G.; Hernandez-Huertas, L.; Abugattas-Nuñez Del Prado, J.; Martinez-Morales, J. R.; DeVore, M. L.; Hassan, H.; Moreno-Sanchez, I.; Tomas-Gallardo, L.; Diaz-Moscoso, A.; Monges, D. E.; Guelfo, J. R.; Theune, W. C.; Brannan, E. O.; Wang, W.; Corbin, T. J.; Moran, A. M.; Sánchez Alvarado, A.; Málaga-Trillo, E.; Takacs, C. M.; Bazzini, A. A.; Moreno-Mateos, M. A. CRISPR-Cas13d Induces Efficient mRNA Knockdown in Animal Embryos. *Dev. Cell* **2020**, *54*, 805−817.e7.
(36) Piepenburg, O.; Williams, C. H.; Stemple, D. L.; Armes, N. A. DNA Detection Using Recombination Proteins. *PLoS Biol.* **2006**, *4*, No. e204.

https://doi.org/10.1021/acssensors.1c01088
ACS Sens. XXXX, XXX, XXX−XXX

(37) Corman, V. M.; Landt, O.; Kaiser, M.; Molenkamp, R.; Meijer, A.; Chu, D. K. W.; Bleicker, T.; Brünink, S.; Schneider, J.; Schmidt, M. L.; Mulders, D. G. J. C.; Haagmans, B. L.; van der Veer, B.; van den Brink, S.; Wijsman, L.; Goderski, G.; Romette, J.-L.; Ellis, J.; Zambon, M.; Peiris, M.; Goossens, H.; Reusken, C.; Koopmans, M. P. G.; Drosten, C. Detection of 2019 Novel Coronavirus (2019-nCoV) by Real-Time RT-PCR. *Eurosurveillance* **2020**, *25*, No. 2000045.
(38) Lu, X.; Wang, L.; Sakthivel, S. K.; Whitaker, B.; Murray, J.; Kamili, S.; Lynch, B.; Malapati, L.; Burke, S. A.; Harcourt, J.; Tamin, A.; Thornburg, N. J.; Villanueva, J. M.; Lindstrom, S. US CDC Real-Time Reverse Transcription PCR Panel for Detection of Severe Acute Respiratory Syndrome Coronavirus 2. *Emerging Infect. Dis.* **2020**, *26*, No. 1654.
(39) Broughton, J. P.; Deng, X.; Yu, G.; Fasching, C. L.; Singh, J.; Streithorst, J.; Granados, A.; Sotomayor-Gonzalez, A.; Zorn, K.; Gopez, A.; Hsu, E.; Gu, W.; Miller, S.; Pan, C.-Y.; Guevara, H.; Wadford, D.; Chen, J.; Chiu, C. Y. Rapid Detection of 2019 Novel Coronavirus SARS-CoV-2 Using a CRISPR-Based DETECTR Lateral Flow Assay *Infectious Diseases (except HIV/AIDS)* 2020. DOI: 10.1101/2020.03.06.20032334.
(40) Howson, E. L. A.; Kurosaki, Y.; Yasuda, J.; Takahashi, M.; Goto, H.; Gray, A. R.; Mioulet, V.; King, D. P.; Fowler, V. L. Defining the Relative Performance of Isothermal Assays That Can Be Used for Rapid and Sensitive Detection of Foot-and-Mouth Disease Virus. *J. Virol. Methods* **2017**, *249*, 102−110.
(41) Sefers, S.; Schmitz, J. E. Molecular Contamination and Amplification Product Inactivation. In *Advanced Techniques in Diagnostic Microbiology: Volume 1: Techniques*; Tang, Y.-W.; Stratton, C. W., Eds.; Springer International Publishing: Cham, 2018; pp 505−526.
(42) Fozouni, P.; Son, S.; Díaz de León Derby, M.; Knott, G. J.; Gray, C. N.; D'Ambrosio, M. V.; Zhao, C.; Switz, N. A.; Kumar, G. R.; Stephens, S. I.; Boehm, D.; Tsou, C.-L.; Shu, J.; Bhuiya, A.; Armstrong, M.; Harris, A. R.; Chen, P.-Y.; Osterloh, J. M.; Meyer-Franke, A.; Joehnk, B.; Walcott, K.; Sil, A.; Langelier, C.; Pollard, K. S.; Crawford, E. D.; Puschnik, A. S.; Phelps, M.; Kistler, A.; DeRisi, J. L.; Doudna, J. A.; Fletcher, D. A.; Ott, M. Amplification-Free Detection of SARS-CoV-2 with CRISPR-Cas13a and Mobile Phone Microscopy. *Cell* **2021**, *184*, 323−333.e9.
(43) Li, M.; Akbari, O. S.; White, B. J. Highly Efficient Site-Specific Mutagenesis in Malaria Mosquitoes Using CRISPR. *G3: Genes, Genomes, Genet.* **2018**, *8*, 653−658.
(44) Brieba, L. G.; Padilla, R.; Sousa, R. Role of T7 RNA Polymerase His784 in Start Site Selection and Initial Transcription. *Biochemistry* **2002**, *41*, 5144−5149.

https://doi.org/10.1021/acssensors.1c01088
ACS Sens. XXXX, XXX, XXX−XXX